

Prediction of high-temperature ambient-pressure superconductivity in hexagonal boron-rich clathrates

Bin Li,^{1,2,*} Yuxiang Fan,¹ Chuanhui Yin,³ Junjie Zhai,^{1,4} Cong Zhu,³ Zhisi Cao,¹ Jie Cheng,^{1,2} and Shengli Liu¹

¹*School of Science, Nanjing University of Posts and Telecommunications, Nanjing 210023, China*

²*Jiangsu Provincial Engineering Research Center of Low Dimensional Physics and New Energy, Nanjing University of Posts and Telecommunications, Nanjing 210023, China*

³*College of Electronic and Optical Engineering, Nanjing University of Posts and Telecommunications, Nanjing 210023, China*

⁴*Key Laboratory of Dark Matter and Space Astronomy,*

Purple Mountain Observatory, Chinese Academy of Sciences, Nanjing 210023, China

(Dated: March 11, 2025)

Inspired by recent predictions of superconductivity in B-C framework clathrates, we employ density functional theory to explore potential superconductors among hexagonal hydride-substituted compounds with compositions XB_8C , XB_7C_2 , XB_6C_3 , XB_3C_6 , XB_2C_7 , and XBC_8 . Our high-throughput calculations on 96 compounds reveal several dynamically stable candidates exhibiting superconductivity at ambient pressure. Analysis of electronic structures and electron-phonon coupling demonstrates that CaB_8C , SrB_8C , and BaB_8C possess superconducting transition temperatures (T_c) exceeding 50 K, with CaB_8C exhibiting the highest predicted T_c of 77.1 K among all stable compounds studied. These findings expand the family of B-C clathrate superconductors and provide valuable insights for experimental efforts aimed at discovering novel superconducting materials.

I. INTRODUCTION

The concept of “metallic hydrogen” first proposed in 1935 [1], was later expanded by Ashcroft, who predicted its potential for room-temperature superconductivity under high pressure [2]. Ashcroft further suggested that hydrogen-rich materials could achieve high-temperature superconductivity at lower pressures through “chemical pre-compression” [3]. Recent theoretical studies have indicated that hydrogen-based superconductors can exceed room-temperature transition temperatures, with many hydrogen-rich compounds containing main group elements now considered potential high- T_c superconductors. Experimental verifications include H_3S (203 K at 200 GPa) [4], MgH_6 (271 K at 300 GPa) [5], CaH_6 (235 K at 150 GPa) [6], LaH_{10} (280 K at 210 GPa) [7], and CeH_9 (105-117 K at 200 GPa) [8]. However, the extreme pressure conditions exceeding 100 GPa present significant challenges for practical applications [9, 10]. To address this limitation, several ternary hydrides have been reported with more favorable superconducting properties at lower pressures, including LaBeH_8 (110 K at 80 GPa) [11], LaBH_8 (126 K at 50 GPa) [12], CeBeH_8 (56 K at 10 GPa), CeBH_8 (118 K at 150 GPa) [13], and $(\text{La},\text{Y})\text{H}_{10}$ (253 K at 183 GPa) [14] opening new avenues for high-temperature superconductor research and potential applications.

The stability challenges of hydride-rich high-temperature superconductors at low pressures have shifted scientific focus towards boron-carbon/boron-nitride/borosilicide superconductors [15–22], which exhibit stability at low or ambient pressures. Carbon, a fundamental element, forms diverse stable structures

with other elements and itself, as evidenced by superconductivity in graphite intercalation compounds [23], CaC_6 ($T_c = 11.5$ K) [24], and Cs_3C_{60} and $\text{RbCs}_2\text{C}_{60}$ ($T_c = 40$ K and 33 K, respectively) [25, 26]. Boron, with its unique electron-deficient configuration, contributes to versatile bonding in metal borides like MgB_2 , a conventional superconductor with $T_c = 39$ K at atmospheric pressure due to strong electron-phonon coupling [27]. The investigation of boron-carbon bonding networks, including boron-doped diamond [28], SrB_3C_3 [29], Ca-B-C systems [21], KPbB_6C_6 , and $\text{Rb}_{0.4}\text{Sr}_{0.6}\text{B}_3\text{C}_3$ [16, 20], has been motivated by the concept of substituting carbon atoms with boron to stabilize structures [30]. This approach offers a promising avenue for designing superconductors with unique properties, as the prevalence of sp^3 hybridization in these compounds enables strong electron-phonon coupling, enhancing superconductivity while reducing pressure requirements for dynamic stability. The exploration of boron-carbon and boron-nitrogen frameworks, driven by their inherent structural stability and potential for low-pressure high- T_c superconductivity, represents a promising frontier in condensed matter physics and materials science.

Building upon previous research [8, 31], we propose an approach to superconductivity by substituting hydrogen with boron and carbon elements, aiming to achieve high-temperature superconductivity at lower pressures. Our theoretical study focuses on the stoichiometry of B and C, emphasizing compound stability under atmospheric conditions and the potential for high- T_c superconductivity. Using first-principles calculations, we investigate the electronic band structure, phonon spectrum, electron-phonon interaction, and T_c of compounds with the general formula XB_8C at ambient pressure, where X represents Ca, Ba, or Sr. Notably, our findings predict a T_c of 77.1 K for CaB_8C at ambient pressure, significantly expanding the potential of B-C framework inclusion com-

* Electronic addresses: libin@njupt.edu.cn

plexes in the field of superconductivity. This work not only explores a new class of superconducting materials but also provides insights into the fundamental mechanisms underlying high-temperature superconductivity in non-hydride systems, potentially paving the way for the design of practical, ambient-pressure superconductors.

II. METHODS

Electronic bands, density of states, and Fermi surfaces were calculated using the WIEN2K package, which implements the full potential linear augmented plane wave (FP-LAPW) method with local orbitals [32, 33]. The Pedrew-Burke-Ernzerhof form of the generalized gradient approximation (GGA) was chosen for the exchange-correlation functional, providing values closer to experimental results. Phonon and electron-phonon coupling matrix elements were computed using density functional perturbation theory (DFPT) [34], with pseudopotentials selected from the standard solid-state pseudopotential (SSSP) library [35]. The Quantum-Espresso (QE) package, utilizing the pseudopotential plane wave method, was employed within the DFPT framework to obtain detailed structural information [36]. Self-consistent calculations used a plane wave basis set with charge density and wave function cutoffs of 600 Ry and 60 Ry, respectively. Convergence was achieved using a $6 \times 6 \times 6$ high-symmetry q -point grid and a $12 \times 12 \times 12$ k -point grid for crystal structure optimization and total energy estimation. Efficient materials calculations employed dense $24 \times 24 \times 24$ Monkhorst-Pack special points [37], while Brillouin zone (BZ) integration utilized the tetrahedron method [38]. Crystal structure modeling and visualization were performed using VESTA [39], with Fermi surface analysis conducted using XCRYSDEN and FermiSurfer tools [40]. To characterize the superconducting properties of the most promising candidate materials, we employed the Eliashberg spectral function $\alpha^2 F(\omega)$, which effectively represents the electron-phonon coupling in conventional superconductivity:

$$\alpha^2 F(\omega) = \frac{1}{2\pi N(E_f)} \sum_{Q\nu} \frac{\gamma_{Q\nu}}{\hbar\omega_{Q\nu}} \delta(\omega - \omega_{Q\nu}), \quad (1)$$

where $N(E_f)$ is density of states at the Fermi level, $\gamma_{Q\nu}$ is the electron-phonon line width, and $\omega_{Q\nu}$ is the phonon frequency at phonon branch ν and wavevector Q . The electron-phonon coupling constant λ is obtained by integrating $\alpha^2 F(\omega)$ and is written as:

$$\lambda = \sum_{Q\nu} \lambda_{Q\nu} = 2 \int_0^\omega d\omega \alpha^2 F(\omega) / \omega, \quad (2)$$

where ω_{log} is the logarithmic average phonon frequency, expressed as:

$$\omega_{log} = \exp\left[\frac{2}{\lambda} \int_0^\infty \frac{d\omega}{\omega} \alpha^2 F(\omega) \log(\omega)\right]. \quad (3)$$

The approximate estimation of the transition temperature is obtained using the Allen-Dynes modified McMillan (ADM) formula. Typically, the predicted critical temperature closely aligns with the critical temperature derived from the solution of the Eliashberg equations [41]. The ADM equation is as follows:

$$T_c = f_1 f_2 \frac{\omega_{log}}{1.2} \exp\left[-\frac{1.04(1 + \lambda)}{\lambda - \mu^*(1 + 0.62\lambda)}\right], \quad (4)$$

The Coulomb pseudopotential constant μ^* is set to 0.1 in these calculations. The factor f_1 accounts for strong coupling corrections, while the factor f_2 represents shape correction. The values of these factors, f_1 and f_2 , are determined by the parameters λ , μ^* , ω_{log} , and $\bar{\omega}_2$. The expressions for these factors are given by:

$$f_1 = \sqrt[3]{1 + \left(\frac{\lambda}{2.46(1 + 3.8\mu^*)}\right)^{\frac{3}{2}}} \quad (5)$$

$$f_2 = 1 + \frac{(\bar{\omega}_2/\omega_{log} - 1)\lambda^2}{\lambda^2 + 3.312(1 + 6.3\mu^*)^2(\bar{\omega}_2/\omega_{log})^2} \quad (6)$$

III. RESULTS AND DISCUSSION

Prior to analyzing the stability of ternary compounds in the boron-carbon system at ambient pressure, we evaluated their structural properties by substituting hydrogen atoms in CeH_9 with boron and carbon atoms, using the known $P6_3/mmc$ (space group No. 194) structure as a reference [8]. This substitution results in six compound configurations: XB_8C , XB_7C_2 , XB_6C_3 , XB_3C_6 , XB_2C_7 , and XBC_8 . We evaluated 16 potential X atoms ($X = \text{Li}, \text{Na}, \text{K}, \text{Rb}, \text{Cs}, \text{Be}, \text{Mg}, \text{Ca}, \text{Sr}, \text{Ba}, \text{Al}, \text{Sc}, \text{Y}, \text{La}, \text{Lu},$ and Ce). The characteristics of these compounds exhibit substantial variation based on the precise chemical composition of boron and carbon atoms. Through extensive high-throughput computational screening, we systematically explored all potentially stable compounds. Subsequent electron-phonon coupling calculations further narrowed our focus to the elements Ca, Sr, and Ba, as their XB_8C compounds exhibit electron-phonon coupling constants greater than 1. We examined the decomposition enthalpies of XB_8C ($X = \text{Ca}, \text{Sr}, \text{Ba}$) in the pressure range of 0 to 120 GPa and found that above 40 GPa, CaB_8C transitions from the decomposition state of $\text{Ca} + 8\text{B} + \text{C}$, and SrB_8C transitions from the decomposition state of $\text{Sr} + \text{B}_4\text{C} + 4\text{B}$. Several additional synthesis routes were identified: $\frac{1}{2}\text{B}_4\text{C} + \text{Ca} + 6\text{B} + \frac{1}{2}\text{C} \xrightarrow{45 \text{ GPa}}$ CaB_8C , $\frac{1}{6}\text{CaC}_6 + \frac{5}{6}\text{CaB}_6 + 3\text{B} \xrightarrow{60 \text{ GPa}}$ CaB_8C , $\text{Sr} + 8\text{B} + \text{C} \xrightarrow{30 \text{ GPa}}$ SrB_8C , $\frac{1}{6}\text{SrC}_6 + \frac{5}{6}\text{Sr} + 8\text{B} \xrightarrow{35 \text{ GPa}}$ SrB_8C , $\frac{1}{4}\text{SrB}_2\text{C}_2 + \frac{3}{4}\text{Sr} + \frac{15}{2}\text{B} + \frac{1}{2}\text{C} \xrightarrow{55 \text{ GPa}}$ SrB_8C , $\frac{1}{6}\text{BaC}_6 + \frac{5}{6}\text{Ba} + 8\text{B} \xrightarrow{13 \text{ GPa}}$ BaB_8C , $\text{Ba} + 8\text{B} + \text{C} \xrightarrow{120 \text{ GPa}}$ BaB_8C ,

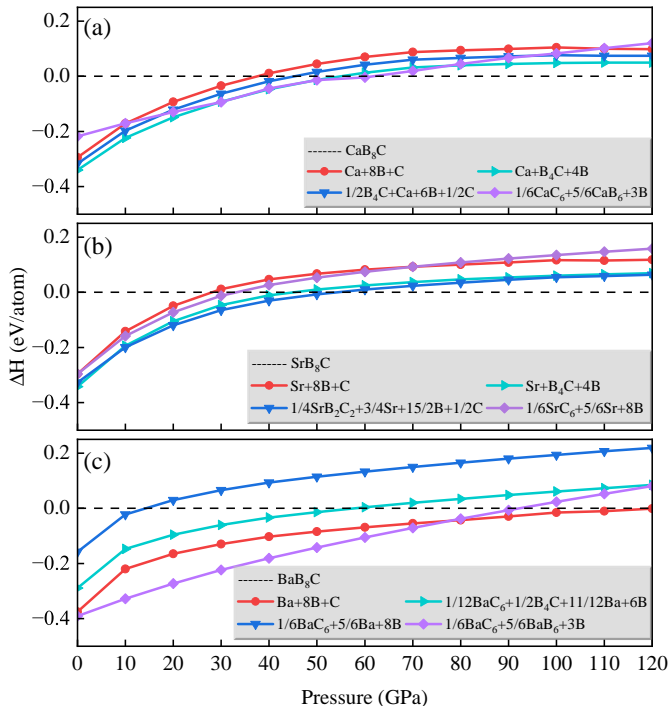


FIG. 1. The relationship between the CaB_8C , SrB_8C and BaB_8C structure and the enthalpy difference of the different products of decomposition is calculated for pressures ranging from 0 to 120 GPa.

as illustrated in Fig. 1. The decomposition products were primarily identified from structures examined in the Open Quantum Materials Database (OQMD) [42], including CaC_6 [43], CaB_6 [44], B_4C [45], and BaB_6 [46]. This comprehensive analysis of structural stability and pressure-dependent synthesis routes provides crucial insights into the behavior of CaB_8C , SrB_8C and BaB_8C , laying the foundation for subsequent investigations of its potential superconducting properties.

Figure 2(a) depicts the optimized hexagonal structure of the CaB_8C unit cell in the $P6_3/mmc$ space group at ambient pressure. Unlike most boron-carbon superconductors, the XB_8C compound studied here exhibits a relatively high concentration of B atoms. In this structure, Ca atoms occupy the Wyckoff position $2d$ ($1/3, 2/3, 1/4$), C atoms are located at $2b$ ($0, 0, 1/4$), and B atoms are distributed at $4f$ ($1/3, 2/3, 0.1499$) and $12k$ ($0.1565, 0.8435, 0.4404$). Figure 2(b) illustrates the boron-carbon cage that encapsulates a central calcium atom. The optimized CaB_8C has lattice constants $a = b = 4.679 \text{ \AA}$ and $c = 7.7596 \text{ \AA}$. Structural optimization of CaB_8C , SrB_8C , and BaB_8C reveals a monotonic increase in the B–C bond length. As the atomic mass and ionic radius of the alkaline earth metal increase along the series $\text{Ca} \rightarrow \text{Sr} \rightarrow \text{Ba}$, the B–C bond length systematically increases from 1.684 \AA in CaB_8C to 1.706 \AA in SrB_8C and further to 1.728 \AA in BaB_8C . The electron localization function (ELF) in

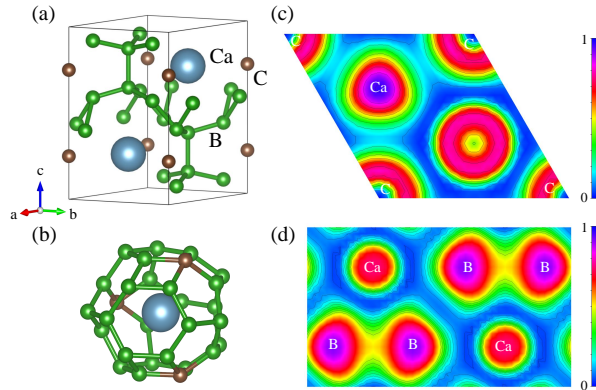


FIG. 2. Structure and electron localization in $P6_3/mmc$ - CaB_8C . (a) Crystal structure of the hexagonal $P6_3/mmc$ phase of CaB_8C . (b) Boron-carbon cage encapsulating a central calcium atom. (c) Calculated ELF in the (001) plane and (d) ELF in the (100) plane.

Figure 2(c,d) illustrates the covalent B–B bonding. Using Bader charge analysis, we quantified the electron transfer for each element in the structure. The analysis reveals that each Ca atom donates 1.409 electrons (charge state: +1.409), contributing a total of 2.818 electrons to the B–C cage. Within the boron framework, four B atoms act as electron acceptors while twelve B atoms serve as donors. Each C atom gains an average of 3.658 electrons, resulting in a formal charge of -3.658. Detailed Bader charge analysis for each element can be found in Table S1 of the supplementary material[53].

The electronic structure and physical properties of B–C inclusion complexes can be tailored by incorporating different guest atoms. We conducted a detailed investigation into the electronic band structure and density of states (DOS) for atoms in the boron-rich compound XB_8C , where X represents Ca, Sr, and Ba. These compounds exhibit similar band structure characteristics, as shown in Fig. 3. All compounds exhibit metallic characteristics, with four bands intersecting the Fermi level (E_F) along high-symmetry paths. These bands can be categorized into two distinct groups: (i) bands 1 and 2 show high degeneracy along the Γ - A - H - K and L - H paths, and (ii) bands 3 and 4 similarly exhibit degeneracy along these paths. Notably, we observed asymmetric band dispersions along the Γ - A - H path: while the bands show linear behavior when approaching from the Γ direction (Γ - A), they deviate from linearity when approaching from the H direction (H - A). The observed band structure configuration exhibits a compelling interplay of flat and dispersive bands near the Fermi level (E_F), a characteristic often associated with enhanced superconductivity [47]. Particularly noteworthy is the presence of a flat band near E_F along the K - Γ - M and L - H paths, coexisting with steep bands that cross E_F along Γ - A . This unique combination of band features is es-

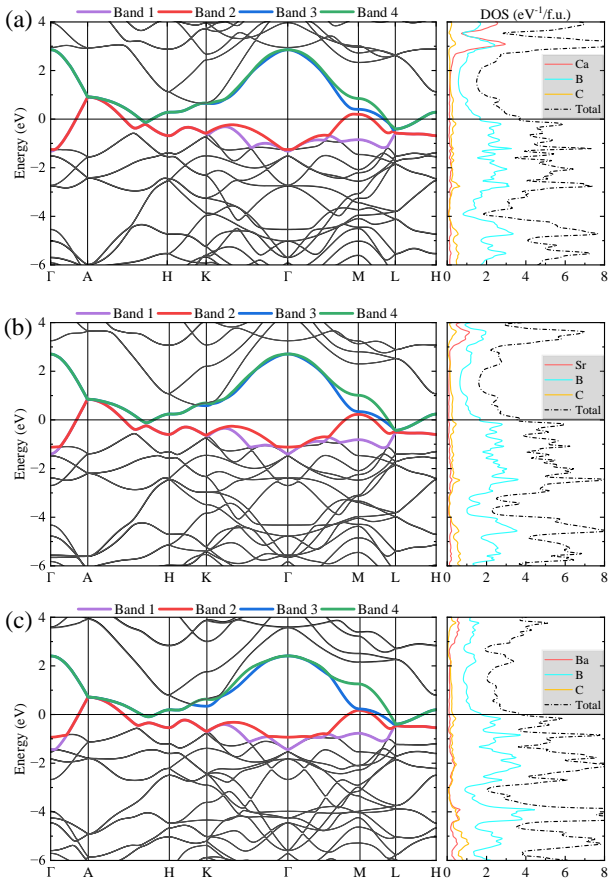


FIG. 3. Electronic band structure and projected density of states (DOS) for the $P6_3/mmc$ structure at ambient pressure for (a) CaB_8C , (b) SrB_8C , and (c) BaB_8C . The band structures (left panels) are illustrated along high-symmetry paths in the Brillouin zone, highlighting four bands that cross the Fermi level (E_F). The corresponding DOS (right panels) reveal the contributions from individual atomic species, providing insight into the electronic properties of each compound. The E_F is normalized to zero energy and is indicated by the solid horizontal line.

pecially significant, as it can lead to an increased density of states at E_F and potentially stronger electron-phonon coupling. The flat band may contribute to a higher effective mass of charge carriers, while the steep bands can facilitate efficient charge transport. Such a band structure is conducive to the formation of Cooper pairs and could potentially result in a higher superconducting transition temperature. Analysis of the DOS reveals that the DOS for C and alkaline earth metal atoms remains relatively low. Conversely, B atoms contribute significantly more to the DOS at the Fermi level, indicating that the metallicity of these compounds primarily originates from the B atoms. This comprehensive analysis of the electronic structure provides crucial insights into the potential superconducting behavior of these boron-rich compounds and the role of different atomic species in determining their electronic properties.

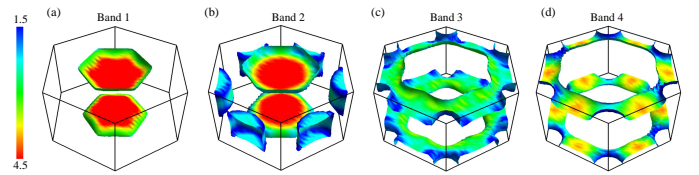


FIG. 4. Fermi surface topology of $P6_3/mmc$ - CaB_8C at ambient pressure. (a–d) Four distinct sheets of the Fermi surface, corresponding to the bands crossing the Fermi level. The color scale represents the magnitude of the Fermi velocity $|\mathbf{v}_F|$, with red indicating high velocities and blue indicating low velocities.

A detailed visualization of the Fermi surfaces for CaB_8C at ambient pressure is presented in Figure 4. The surfaces are color-coded to illustrate the distribution of Fermi velocity, with a gradient transitioning from blue to red as the velocity increases. This intricate Fermi surface topology comprises four distinct components: (i) Two pan-like surfaces located around the A point at the top and bottom center of the BZ, exhibiting strong Fermi velocity at their centers; (ii) A similar structure to band 1, but featuring six additional bowl-shaped sheets located at the side faces of the hexagonal BZ; (iii) Flat, belt-like sheets extending across the top and bottom of the BZ; (iv) A structure akin to band 3, albeit characterized by different Fermi velocity distributions. Together, these components illustrate the complex electronic behavior of CaB_8C , highlighting the significance of Fermi surface topology in understanding its electronic properties.

Further analysis focused on the phonon and electron-phonon coupling interactions of CaB_8C , SrB_8C , and BaB_8C . The calculations for XB_8C yield 40 phonon branches, classified at the Γ point according to the irreducible representation $D_{6h} = 3A_{1g} \oplus A_{1u} \oplus A_{2g} \oplus 5A_{2u} \oplus 5B_{1g} \oplus B_{1u} \oplus B_{2g} \oplus 3B_{2u} \oplus 4E_{2u} \oplus 6E_{2g} \oplus 6E_{1u} \oplus 4E_{1g}$, where $\Gamma_{\text{acoustic}} = A_{2u} \oplus E_{1u}$. As shown in Fig. 5(a), the phonon dispersion at 0 GPa exhibits no imaginary frequencies, confirming dynamic stability. From Ca to Sr to Ba, we observe decreasing lattice vibrations and reduced maximum frequency in the phonon spectrum. The low-frequency branch ($<200 \text{ cm}^{-1}$) is predominantly influenced by X atom vibrations, while the high-frequency optical branch ($>200 \text{ cm}^{-1}$) relates to B and C atom vibrations. Phonon dispersion calculations reveal strong electron-phonon coupling for CaB_8C along the K - Γ - M path, particularly near 100 cm^{-1} . SrB_8C shows significant coupling at both K and M points across 0 – 500 cm^{-1} , whereas BaB_8C 's coupling is mainly in the optical branches. The Eliashberg function $\alpha^2F(\omega)$ shows alkaline earth atom vibrations contributing to the acoustic mode and low-frequency density peak, while B and C vibrations affect the high-frequency optical branches. The detailed superconducting properties of several stable compounds are listed in Table I. Superconducting

	λ	ω_{log} (K)	$\overline{\omega_2}$ (K)	ADM T_c (K)	Eliashberg T_c (K)
CaB ₈ C	1.715	490	702	77.1	83.9
SrB ₈ C	1.416	522	687	64.4	68.9
BaB ₈ C	1.244	506	681	53.2	55.8
RbBC ₈	0.546	831	1008	14.4	15.4
NaB ₆ C ₃	0.512	694	893	9.5	10.6
BaB ₇ C ₂	0.628	590	741	15.9	17.1
SrB ₇ C ₂	0.617	620	788	16.0	16.9

TABLE I. Several compounds exhibiting T_c exceeding 10 K are compared based on their electron-phonon coupling strength λ , the logarithmic average of phonon frequency ω_{log} , the root-mean-square frequency $\overline{\omega_2}$, and the calculated T_c . The T_c values are obtained from both the Allen-Dynes modified McMillan equation and the Eliashberg equation, with a Coulomb pseudopotential of $\mu^* = 0.1$.

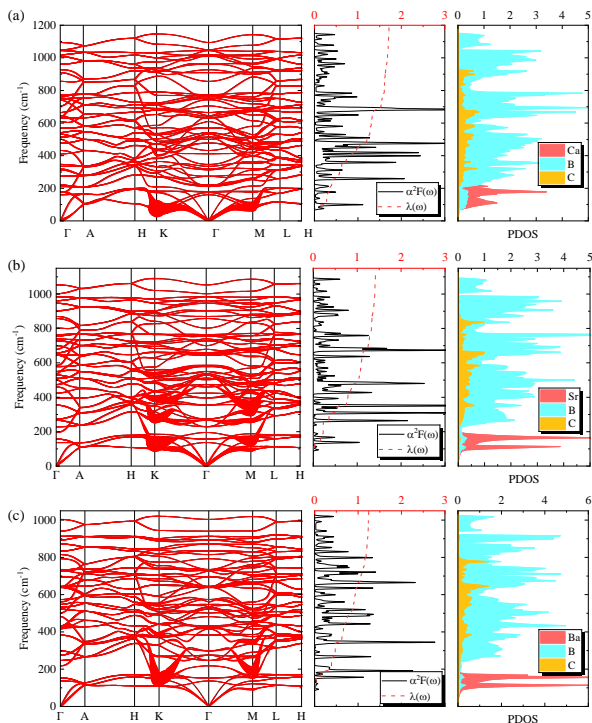


FIG. 5. Phonon dispersions at ambient pressure for (a) CaB₈C, (b) SrB₈C, and (c) BaB₈C. The phonon frequencies ω_{qv} are depicted as black solid lines, while the color scale indicates the electron-phonon coupling strength λ_{qv} , represented by red circles. The middle panels present the Eliashberg spectral function $\alpha^2F(\omega)$ and the electron-phonon coupling strength $\lambda(\omega)$. The right panel displays the phonon density of states (PDOS) projected onto specific atomic species. In this diagram, contributions from Ca, Sr, and Ba are illustrated in red, while those from B and C are shown in cyan and yellow, respectively, facilitating clear differentiation of the atomic contributions to the phonon spectrum.

λ values for CaB₈C, SrB₈C, and BaB₈C (1.715, 1.416, and 1.244, respectively) are primarily determined by high-frequency modes, decreasing with increasing atomic number of alkaline earth metals. The logarithmic average phonon frequency ω_{log} of CaB₈C is 490 K. Using a

Coulomb pseudopotential μ^* of 0.1, the T_c is estimated at 77.1 K (Allen-Dynes modified McMillan equation) and 83.9 K (Eliashberg equation). SrB₈C and BaB₈C exhibit slightly lower T_c due to low-frequency vibrations of heavier alkaline earth metal atoms. We present the superconducting properties of additional X-B-C compounds (RbBC₈, NaB₆C₃, BaB₇C₂, and SrB₇C₂), as summarized in Table I. These materials exhibit moderate electron-phonon coupling constants ranging from 0.51 to 0.63, resulting in predicted superconducting transition temperatures between 10 and 20 K, suggesting their potential as moderate-temperature superconductors within the X-B-C family. Our findings on SrB₇C₂ align with a recent study by Zhang et al. [48], further corroborating the potential of boron-carbon based compounds in high-temperature superconductivity research. Furthermore, the enrichment of boron increases the likelihood that the compounds will remain kinetically stable at ambient pressure while also enhancing the potential for higher superconducting transition temperatures. Compared to ω_{log} , the λ value has a more significant impact on T_c . For example, RbBC₈, a compound with a high ω_{log} of 831 K, has a T_c of about 15 K, much lower than that of the XB₈C compounds. Consequently, three compounds with the highest boron enrichment: CaB₈C, SrB₈C, and BaB₈C have drawn our attention due to their higher λ values and the correspondingly high calculated T_c values. The phonon spectra for all other investigated compositions, encompassing both stable and unstable compounds, along with the additional anharmonic effects on the phonon spectra of XB₈C by combining the Stochastic Self-Consistent Harmonic Approximation (SSCHA) method [49–52], are detailed in the Supplementary Material [53].

IV. CONCLUSION

In this study, we employed first-principles methods to investigate the substitution of hydrides with hexagonal $P6_3/mmc$ -structured B-C compounds, focusing on alkaline earth metal-boron-carbon inclusion complexes of the form XB₈C. Our comprehensive analysis encompassed stability, electronic structure, dynamic proper-

ties, and electron-phonon coupling interactions. While all examined compounds exhibit metastability under ambient conditions, CaB_8C notably becomes energetically favorable relative to its dissociated elements above 40 GPa, suggesting potential high-pressure synthesis routes. Electron-phonon coupling calculations reveal that XB_8C ($X = \text{Ca}, \text{Sr}, \text{Ba}$) compounds maintain dynamic stability at 0 GPa and show promise as high-temperature superconductors, with CaB_8C predicted to have a superconducting transition temperature of 77.1 K at ambient pressure. These findings provide a robust foundation for further theoretical and experimental exploration of clathrate superconductors within the B-C framework, potentially opening new avenues for the design and synthesis of novel superconducting materials with enhanced properties and ambient condition stability. Future research di-

rections may include investigating pressure-induced synthesis techniques, exploring doping strategies to further enhance T_c , and examining the potential of other metal-boron-carbon compositions for superconductivity.

ACKNOWLEDGMENTS

This work is supported by the National Natural Science Foundation of China (Grants No. 12175107, 11504182), the Hua Li Talents Program of Nanjing University of Posts and Telecommunications, and the Natural Science Foundation of Nanjing University of Posts and Telecommunications (Grants No. NY224165, NY219087, NY220038).

-
- [1] E. Wigner and H. B. Huntington, On the possibility of a metallic modification of hydrogen, *The Journal of Chemical Physics* **3**, 764 (1935).
- [2] N. W. Ashcroft, Metallic hydrogen: a high-temperature superconductor? *Phys. Rev. Lett.* **21**, 1748 (1968).
- [3] N. W. Ashcroft, Hydrogen dominant metallic alloys: high temperature superconductors? *Phys. Rev. Lett.* **92**, 187002 (2004).
- [4] A. P. Drozdov, M. I. Erements, I. A. Troyan, V. Ksenofontov, and S. I. Shylin, Conventional superconductivity at 203 kelvin at high pressures in the sulfur hydride system, *Nature* **525**, 73 (2015).
- [5] X. Feng, J. Zhang, G. Gao, H. Liu, and H. Wang, Compressed sodalite-like MgH_6 as a potential high-temperature superconductor, *RSC Adv.* **5**, 59292 (2015).
- [6] H. Wang, J. S. Tse, K. Tanaka, T. Iitaka, and Y. Ma, Superconductive sodalite-like clathrate calcium hydride at high pressures, *Proceedings of the National Academy of Sciences* **109**, 6463 (2012).
- [7] A. P. Drozdov, P. P. Kong, V. S. Minkov, S. P. Besedin, M. A. Kuzovnikov, S. Mozaffari, L. Balicas, F. F. Balakirev, D. E. Graf, V. B. Prakapenka, E. Greenberg, D. A. Knyazev, M. Tkacz, and M. I. Erements, Superconductivity at 250 K in lanthanum hydride under high pressures, *Nature* **569**, 528 (2019).
- [8] N. P. Salke, M. M. Davari Esfahani, Y. Zhang, I. A. Kruglov, J. Zhou, Y. Wang, E. Greenberg, V. B. Prakapenka, J. Liu, A. R. Oganov, and J.-F. Lin, Synthesis of clathrate cerium superhydride CeH_9 at 80-100 GPa with atomic hydrogen sublattice, *Nature Communications* **10**, 4453 (2019).
- [9] L. Ma, K. Wang, Y. Xie, X. Yang, Y. Wang, M. Zhou, H. Liu, X. Yu, Y. Zhao, H. Wang, G. Liu, and Y. Ma, High-Temperature Superconducting Phase in Clathrate Calcium Hydride CaH_6 up to 215 K at a Pressure of 172 GPa, *Phys. Rev. Lett.* **128**, 167001 (2022).
- [10] Z. M. Geballe, H. Liu, A. K. Mishra, M. Ahart, M. Somayazulu, Y. Meng, M. Baldini, and R. J. Hemley, Synthesis and Stability of Lanthanum Superhydrides, *Angewandte Chemie International Edition* **57**, 688 (2018).
- [11] Y. Song, J. Bi, Y. Nakamoto, K. Shimizu, H. Liu, B. Zou, G. Liu, H. Wang, and Y. Ma, Stoichiometric Ternary Superhydride LaBeH_8 as a New Template for High-Temperature Superconductivity at 110 K under 80 GPa, *Phys. Rev. Lett.* **130**, 266001 (2023).
- [12] S. Di Cataldo, C. Heil, W. von der Linden, and L. Boeri, LaBH_8 : Towards high- T_c low-pressure superconductivity in ternary superhydrides, *Phys. Rev. B* **104**, L020511 (2021).
- [13] Y. Hou, B. Li, Y. Bai, X. Hao, Y. Yang, F. Chi, S. Liu, J. Cheng, and Z. Shi, Superconductivity in CeBeH_8 and CeBH_8 at moderate pressures, *Journal of Physics: Condensed Matter* **34**, 505403 (2022).
- [14] D. V. Semenov, I. A. Troyan, A. G. Ivanova, A. G. Kvashnin, I. A. Kruglov, M. Hanfland, A. V. Sadakov, O. A. Sobolevskiy, K. S. Pervakov, I. S. Lyubutin, K. V. Glazyrin, N. Giordano, D. N. Karimov, A. L. Vasiliev, R. Akashi, V. M. Pudalov, and A. R. Oganov, Superconductivity at 253 K in lanthanum-yttrium ternary hydrides, *Materials Today* **48**, 18 (2021).
- [15] J.-N. Wang, X.-W. Yan, and M. Gao, High-temperature superconductivity in SrB_3C_3 and BaB_3C_3 predicted from first-principles anisotropic Migdal-Eliashberg theory, *Phys. Rev. B* **103**, 144515 (2021).
- [16] N. Geng, K. P. Hilleke, L. Zhu, X. Wang, T. A. Strobel, and E. Zurek, Conventional High-Temperature Superconductivity in Metallic, Covalently Bonded, Binary-Guest C-B Clathrates, *Journal of the American Chemical Society* **145**, 1696 (2023).
- [17] Z. Cui, X. Zhang, Y. Sun, Y. Liu, and G. Yang, Prediction of novel boron-carbon based clathrates, *Phys. Chem. Chem. Phys.* **24**, 16884 (2022).
- [18] X. Cui, K. P. Hilleke, X. Wang, M. Lu, M. Zhang, E. Zurek, W. Li, D. Zhang, Y. Yan, and T. Bi, RbB_3Si_3 : An Alkali Metal Borosilicide that is Metastable and Superconducting at 1 atm, *The Journal of Physical Chemistry C* **124**, 14826 (2020).
- [19] Y.-L. Hai, H.-L. Tian, M.-J. Jiang, W.-J. Li, G.-H. Zhong, C.-L. Yang, X.-J. Chen, and H.-Q. Lin, Improving T_c in sodalite-like boron-nitrogen compound $\text{M}_2(\text{BN})_6$, *Materials Today Physics* **25**, 100699 (2022).
- [20] T.-T. Gai, P.-J. Guo, H.-C. Yang, Y. Gao, M. Gao, and Z.-Y. Lu, Van Hove singularity induced phonon-mediated superconductivity above 77 K in hole-doped SrB_3C_3 ,

- Phys. Rev. B* **105**, 224514 (2022).
- [21] C. Zhang, H. Tang, C. Pan, H. Jiang, H.-J. Sun, K.-M. Ho, and C.-Z. Wang, Machine learning guided discovery of superconducting calcium borocarbides, *Phys. Rev. B* **108**, 024512 (2023).
- [22] B. Li, Y. Cheng, C. Zhu, J. Cheng, and S. Liu, Superconductivity near 70 K in boron-carbon clathrates MB_2C_8 ($M = \text{Na, K, Rb, Cs}$) at ambient pressure, *Phys. Rev. B* **109**, 184517 (2024).
- [23] Y. Iye and S.-i. Tanuma, Superconductivity of graphite intercalation compounds with alkali-metal amalgams, *Phys. Rev. B* **25**, 4583 (1982).
- [24] N. Emery, C. Hérold, M. d’Astuto, V. Garcia, C. Bellin, J. F. Maréché, P. Lagrange, and G. Louprias, Superconductivity of Bulk CaC_6 , *Phys. Rev. Lett.* **95**, 087003 (2005).
- [25] T. Palstra, O. Zhou, Y. Iwasa, P. Sulewski, R. Fleming, and B. Zegarski, Superconductivity at 40K in cesium doped C_{60} , *Solid State Communications* **93**, 327 (1995).
- [26] K. Tanigaki, T. W. Ebbesen, S. Saito, J. Mizuki, J. S. Tsai, Y. Kubo, and S. Kuroshima, Superconductivity at 33 K in $\text{Cs}_x\text{Rb}_y\text{C}_{60}$, *Nature* **352**, 222 (1991).
- [27] J. Nagamatsu, N. Nakagawa, T. Muranaka, Y. Zenitani, and J. Akimitsu, Superconductivity at 39 K in magnesium diboride, *Nature* **410**, 63 (2001).
- [28] E. A. Ekimov, V. A. Sidorov, E. D. Bauer, N. N. Mel’nik, N. J. Curro, J. D. Thompson, and S. M. Stishov, Superconductivity in diamond, *Nature* **428**, 542 (2004).
- [29] L. Zhu, H. Liu, M. Somayazulu, Y. Meng, P. A. Guíña, T. B. Shiell, C. Kenney-Benson, S. Chariton, V. B. Prakapenka, H. Yoon, J. A. Horn, J. Paglione, R. Hoffmann, R. E. Cohen, and T. A. Strobel, Superconductivity in SrB_3C_3 clathrate, *Phys. Rev. Res.* **5**, 013012 (2023).
- [30] T. Zeng, R. Hoffmann, R. Nesper, N. W. Ashcroft, T. A. Strobel, and D. M. Proserpio, Li-Filled, B-Substituted Carbon Clathrates, *Journal of the American Chemical Society* **137**, 12639 (2015).
- [31] B. Li, Z. Miao, L. Ti, S. Liu, J. Chen, Z. Shi, and E. Gregoryanz, Predicted high-temperature superconductivity in cerium hydrides at high pressures, *Journal of Applied Physics* **126**, 235901 (2019).
- [32] P. Blaha, K. Schwarz, F. Tran, R. Laskowski, G. K. H. Madsen, and L. D. Marks, WIEN2k: An APW+lo program for calculating the properties of solids, *The Journal of Chemical Physics* **152**, 074101 (2020).
- [33] P. Blaha, K. Schwarz, P. Sorantin, and S. Trickey, Full-potential, linearized augmented plane wave programs for crystalline systems, *Computer Physics Communications* **59**, 399 (1990).
- [34] P. Giannozzi, O. Baseggio, P. Bonfà, D. Brunato, R. Car, I. Carnimeo, C. Cavazzoni, S. de Gironcoli, P. Delugas, F. Ferrari Ruffino, A. Ferretti, N. Marzari, I. Timrov, A. Urru, and S. Baroni, Quantum ESPRESSO toward the exascale, *The Journal of Chemical Physics* **152**, 154105 (2020).
- [35] G. Prandini, A. Marrazzo, I. E. Castelli, N. Mounet, and N. Marzari, Precision and efficiency in solid-state pseudopotential calculations, *npj Computational Materials* **4**, 72 (2018).
- [36] P. Giannozzi, S. Baroni, N. Bonini, M. Calandra, R. Car, C. Cavazzoni, D. Ceresoli, G. L. Chiarotti, M. Cococcioni, I. Dabo, A. D. Corso, S. de Gironcoli, S. Fabris, G. Fratesi, R. Gebauer, U. Gerstmann, C. Gougoussi, A. Kokalj, M. Lazzeri, L. Martin-Samos, N. Marzari, F. Mauri, R. Mazzarello, S. Paolini, A. Pasquarello, L. Paulatto, C. Sbraccia, S. Scandolo, G. Sclauzero, A. P. Seitsonen, A. Smogunov, P. Umari, and R. M. Wentzcovitch, QUANTUM ESPRESSO: a modular and open-source software project for quantum simulations of materials, *Journal of Physics: Condensed Matter* **21**, 395502 (2009).
- [37] H. J. Monkhorst and J. D. Pack, Special points for Brillouin-zone integrations, *Phys. Rev. B* **13**, 5188 (1976).
- [38] M. Kawamura, Y. Gohda, and S. Tsuneyuki, Improved tetrahedron method for the Brillouin-zone integration applicable to response functions, *Phys. Rev. B* **89**, 094515 (2014).
- [39] K. Momma and F. Izumi, VESTA 3 for three-dimensional visualization of crystal, volumetric and morphology data, *Journal of Applied Crystallography* **44**, 1272 (2011).
- [40] M. Kawamura, FermiSurfer: Fermi-surface viewer providing multiple representation schemes, *Computer Physics Communications* **239**, 197 (2019).
- [41] P. B. Allen and R. C. Dynes, Transition temperature of strong-coupled superconductors reanalyzed, *Phys. Rev. B* **12**, 905 (1975).
- [42] J. E. Saal, S. Kirklin, M. Aykol, B. Meredig, and C. Wolverton, Materials design and discovery with high-throughput density functional theory: the open quantum materials database (OQMD), *Jom* **65**, 1501 (2013).
- [43] C. Wood, N. Skipper, and M. Gillan, Ca-intercalated graphite as a hydrogen storage material: Stability against decomposition into CaH_2 and graphite, *Journal of Solid State Chemistry* **184**, 1561 (2011).
- [44] L. Pauling and S. Weinbaum, The Structure of Calcium Boride, CaB_6 , *Zeitschrift für Kristallographie-Crystalline Materials* **87**, 181 (1934).
- [45] A. Shamp, E. Zurek, T. Ogitsu, D. E. Fratanduono, and S. Hamel, Properties of B_4C in the shocked state for pressures up to 1.5 TPa, *Physical Review B* **95**, 184111 (2017).
- [46] K. Schmitt, C. Stückl, H. Ripplinger, and B. Albert, Crystal and electronic structure of BaB_6 in comparison with CaB_6 and molecular $[\text{B}_6\text{H}_6]^{2-}$, *Solid state sciences* **3**, 321 (2001).
- [47] A. Simon, Superconductivity and Chemistry, *Angewandte Chemie International Edition in English* **36**, 1788 (1997).
- [48] D. Zhang, M. Bhullar, X. Cui, M. Zhang, H. Wang, and Y. Yao, Emergent superconductivity in clathrate $\text{Sr}(\text{B,C})_9$ at low pressures, *Computational Materials Science* **246**, 113419 (2025).
- [49] L. Monacelli, R. Bianco, M. Cherubini, M. Calandra, I. Errea, and F. Mauri, The stochastic self-consistent harmonic approximation: calculating vibrational properties of materials with full quantum and anharmonic effect, *Journal of Physics: Condensed Matter* **33**, 363001 (2021).
- [50] I. Errea, M. Calandra, and F. Mauri, First-Principles Theory of Anharmonicity and the Inverse Isotope Effect in Superconducting Palladium-Hydride Compounds, *Physical Review Letters* **111**, 177002 (2013).
- [51] I. Errea, M. Calandra, and F. Mauri, Anharmonic free energies and phonon dispersions from the stochastic self-consistent harmonic approximation: Application to platinum and palladium hydrides, *Physical Review B* **89**, 064302 (2014).

- [52] R. Bianco, I. Errea, L. Paulatto, M. Calandra, and F. Mauri, Second-order structural phase transitions, free energy curvature, and temperature-dependent anharmonic phonons in the self-consistent harmonic approximation: Theory and stochastic implementation, [Physical Review B](#) **96**, 014111 (2017).
- [53] See supplemental material at <http://link.aps.org/supplemental/xxxxxx>, which includes calculated Bader charge analysis, phonon spectra for all other X-B-C compounds, and anharmonic results for XB_8C ($X = \text{Ca}, \text{Sr}, \text{Ba}$).